Direct monitoring of fluid saturation using time-lapse full-waveform inversion

Amir Mardan, Bernard Giroux*,INRS-ETE, Gabriel Fabien-Ouellet†, Polytechnique Montréal, and Mohammad Reza Saberi‡, GeoSoftware*

SUMMARY

Monitoring the time-lapse changes in subsurface is an important task for better management of reservoirs. Time-lapse seismic data can be used to estimate these changes efficiently. Full-waveform inversion (FWI) has been employed as a powerful technique to recover the (visco)elastic properties of subsurface. Although numerous studies have been carried out using this method for reservoir monitoring, the crosstalk between parameters makes multiparameter time-lapse FWI very challenging. In this study, we use Gassmann's equation to perform time-lapse FWI with a parameterization that could reduce the crosstalk in time-lapse studies. We present the required equations for performing FWI based on porosity, clay content, and water saturation (PCS) parameterization. By implementing the FWI algorithms with PCS parameterization, we show the feasibility of multiparameter time-lapse FWI with a synthetic time-lapse experiment based on the Marmousi model.

INTRODUCTION

Monitoring reservoirs either for oil and gas applications or for the purpose of CO_2 sequestration is a vital task for safe and optimal reservoir management. Time-lapse seismic data have been successfully used for this purpose (Lumley, 1995; Lang and Grana, 2019; Landrø et al., 2003). Due to the ability of full-waveform inversion (FWI) to recover high-resolution images of the subsurface, time-lapse full-waveform inversion (TL-FWI) can be used to process time-lapse seismic surveys (Fabien-Ouellet et al., 2017; Zhou and Lumley, 2021; Mardan et al., 2022b). However, these studies monitor variation of the (visco)elastic properties (V_P, V_S, ρ, Q) to quantify the changes in the subsurface. To obtain the rock-physical changes, usually a two-steps inversion approach is used: to first invert for the elastic properties and then use a rock-physics model to convert the changes to rock-physical properties (Queißer and Singh, 2013; Dupuy et al., 2016).

Elastic FWI needs three elastic properties to model the seismic wavefield. Density plus P- and S-wave velocities (DV) construct the most common parameterization for FWI studies (Queißer and Singh, 2013; Dupuy et al., 2016; Fabien-Ouellet et al., 2017; Zhou and Lumley, 2021; Mardan et al., 2022b). Ma et al. (2016) showed that the DV parameterization is not ideal for TL-FWI. This is due to the fact that changing the saturation of fluids in reservoirs alters all three parameters used for elastic FWI. For example, replacing water with gas, decreases the density and increases the S-wave velocity as shear modulus (μ) does not change with fluid replacement. As a result of gas replacing water, bulk modulus (K) decreases and consequently, P-wave velocity decreases. To address this problem and inspired by Hu et al. (2021), we undertake the TL-FWI using PCS parameterization (porosity, clay content, water saturation). With the PCS parameterization, it can be assumed that the differences between baseline and monitor data are only as a result of changes in water saturation. This assumption is true as we can assume porosity and clay content do not change with fluid replacement. Performing the FWI with PCS parameterization requires rock-physical models as a link between elastic and rock-physics properties (Mavko et al., 2020). We use Gassmann's model (Gassmann, 1951) for this purpose.

In this study, we first present the theory of FWI and TL-FWI in the PCS parameterization. We then test the method on a section of the Marmousi model.

THEORY

Full-waveform inversion

The cost function for time-domain FWI is given by

$$J(\mathbf{m}) = \frac{1}{2}\|\mathbf{R}F(\mathbf{m},\mathbf{u}) - \mathbf{d}\|_2^2, \tag{1}$$

where $\mathbf{R}$ is the measurement operator that maps the wavefield ($\mathbf{u}$) to the receivers' location. The vectors $\mathbf{m}$ and $\mathbf{d}$ are the model parameter and observed seismic data. Three parameters are required to describe an isotropic elastic Earth (Tarantola, 1986). The choice of density and Lamé parameters (λ and μ) is the easiest option as they appear in the wave equation, however the wave equation can be rewritten using density and wave velocities,

$$\begin{cases} \rho \dot{v}_x = \partial_x \tau_{xx} + \partial_z \tau_{xz}, \\ \rho \dot{v}_z = \partial_z \tau_{zz} + \partial_x \tau_{xz}, \\ \dot{\tau}_{xx} = \rho V_P^2 \partial_x v_x + \rho (V_P^2 - 2V_S^2)\partial_z v_z + s, \\ \dot{\tau}_{zz} = \rho (V_P^2 - 2V_S^2)\partial_x v_x + \rho V_P^2 \partial_z v_z + s, \\ \dot{\tau}_{xz} = \rho V_S^2 (\partial_z v_x + \partial_x v_z), \end{cases} \tag{2}$$

where s is the source function and the particle velocities in x- and z-directions (v_x and v_z) in addition to normal (τ_{xx} and τ_{zz}) and shear stresses (τ_{xz}) build the wavefield vector. As Tarantola (1986) has shown, the results of different parameterizations are not equivalent. Hence, with the objective of monitoring fluid saturation in reservoirs, we use Gassmann's equation to develop a more suitable parameterization. First, the bulk and shear moduli of solid frame are obtained by using a general consolidation parameter cs as (Pride, 2005),

$$K_D = K_s \frac{1-\phi}{1+cs\phi}, \qquad \mu_D = \mu_s \frac{1-\phi}{1+\frac{3}{2}cs\phi}. \tag{3}$$

Then, the Gassmann's equation is used to relate porosity (ϕ), bulk moduli of the minerals (K_s), frame (K_D), fluid (K_f), and saturated rock,

$$K = \frac{\phi K_D + (1-(1+\phi)K_D/K_s)K_f}{\phi(1+\Delta)}, \qquad \mu = \mu_D, \qquad \rho = (1-\phi)\rho_s + \phi\rho_f, \tag{4}$$

where

$$\Delta = \frac{1-\phi}{\phi}\frac{K_f}{K_s}\left(1-\frac{1}{1+cs\phi}\right). \tag{5}$$

The properties of fluid (K_f, μ_f, ρ_f) and minerals (K_s, μ_s, ρ_s) can be estimated by weighted arithmetic average,

$$M_f = \sum M_i S_i, \qquad i \in [w,h] \qquad M_s = \sum M_j V_j, \qquad j \in [\text{Clay}, \text{Quartz}] \tag{6}$$

where S and V denote the fluid saturation and the volume of each mineral in the rock, respectively. The subscripts w and h denote the parameters for water and hydrocarbon, respectively. The elastic properties can be calculated using equation 4 as

$$V_P = \sqrt{\frac{K+\frac{4}{3}\mu}{\rho}}, \qquad V_S = \sqrt{\frac{\mu}{\rho}}, \qquad \rho = \rho. \tag{7}$$

For more details on porous media homogenization, readers are referred to the comprehensive study of Dupuy et al. (2016).

To minimize the cost function (equation 1), we need to estimate its gradient with respect to each parameter. In this study, the FWI is performed using PyFWI (Mardan et al., 2022a) which is an open source Python package with the benefit of GPU programming (Fabien-Ouellet et al., 2017). This package provides the gradient of cost function with respect to (V_P, V_S, ρ). Thanks to chain rule, we can obtain the gradient with respect to a given parameter P as

$$\frac{\partial \chi}{\partial P} = \underbrace{\begin{bmatrix} \frac{\partial \chi}{\partial V_P} & \frac{\partial \chi}{\partial V_S} & \frac{\partial \chi}{\partial \rho} \end{bmatrix}}_{\mathbf{J}} \underbrace{\begin{bmatrix} \frac{\partial V_P}{\partial K} & \frac{\partial V_P}{\partial \mu} & \frac{\partial V_P}{\partial \rho} \\ \frac{\partial V_S}{\partial K} & \frac{\partial V_S}{\partial \mu} & \frac{\partial V_S}{\partial \rho} \\ \frac{\partial \rho}{\partial K} & \frac{\partial \rho}{\partial \mu} & \frac{\partial \rho}{\partial \rho} \end{bmatrix}}_{\mathbf{b}} \begin{bmatrix} \frac{\partial k}{\partial P} \\ \frac{\partial \mu}{\partial P} \\ \frac{\partial \rho}{\partial P} \end{bmatrix}, \tag{8}$$

where, based on equation 7,

$$\mathbf{J} = \begin{bmatrix} \frac{1}{2\rho V_P}, & \frac{2}{3\rho V_P}, & -\frac{V_P}{2\rho} \\ 0 & \frac{1}{2\rho V_S} & -\frac{V_S}{2\rho} \\ 0 & 0 & 1 \end{bmatrix}, \tag{9}$$

and P can be taken as one of ϕ, C, or S_w (Appendix A).

Time-lapse full-waveform inversion

Maharramov and Biondi (2014) proposed simultaneous TL-FWI by introducing the cost function

$$\chi(\mathbf{m}_b, \mathbf{m}_m) = \lambda_b \|\mathbf{R}F(\mathbf{m}_b, \mathbf{u}_b) - \mathbf{d}_b\|_2^2 + \lambda_m \|\mathbf{R}F(\mathbf{m}_m, \mathbf{u}_m) - \mathbf{d}_m\|_2^2 + \lambda_\Delta \|\mathbf{m}_m - \mathbf{m}_b\|_2^2, \tag{10}$$

where subscripts b and m denote the baseline and monitor models. This cost function contains three terms: the first term is for inversion of baseline data, the second term inverts the monitor data, and the third term regularizes the optimization based on the difference between two models. Assuming that the cause of any changes in reservoirs is variation of the saturation, we tackle the TL-FWI problem with first updating the initial model by inverting the baseline data and then the recovered porosity and clay content are kept constant in equation 10. Hence, for TL-FWI, only saturation is updated ($\mathbf{m}_b$ and $\mathbf{m}_m$ correspond to saturation of baseline and monitor).

NUMERICAL ANALYSIS

In this section we analyze the feasibility of the proposed method with a section of the Marmousi model. Figure 1(a-f) shows the baseline and monitor models in PCS parameterization. As is shown, the water saturation of a reservoir in the study area is increased by 0.08 or 25%. Converting this model to DV parameterization using the information provided in Table 1, the baseline and monitor models are presented in Figure 2(a-f). Comparing the time-lapse changes in each parameterization (Figure 1(g-i) and Figure 2(g-i)), the challenges of TL-FWI with DV parameterization are clear. By performing the TL-FWI with DV parameterization, the changes in water saturation affect all three elastic parameters. Ma et al. (2016) showed that for multiparameter acoustic case (two parameters), the DV parameterization is seriously affected by the crosstalk between the parameters in baseline with the ones in monitor model. By using the PCS parameterization, we can assign all time-lapse changes between baseline and monitor data to the water saturation and avoid the challenges of multiparameter TL-FWI.

	Bulk modulus (GPa)	Shear modulus (GPa)	Density (g/cm^3)
Quartz	37.00	44.00	2.65
Clay	21.00	10.0	2.55
Water	2.25	0.00	1.00
Gas	0.04	0.00	0.10

Table 1: Elastic properties for minerals and fluids used in this study (Hu et al., 2021).

This study is undertaken by using 7 sources on the surface and placing receivers both on the surface and imaginary wells on both sides of the model. A Ricker wavelet with a central frequency of 30 Hz is used as the source while the inversion is

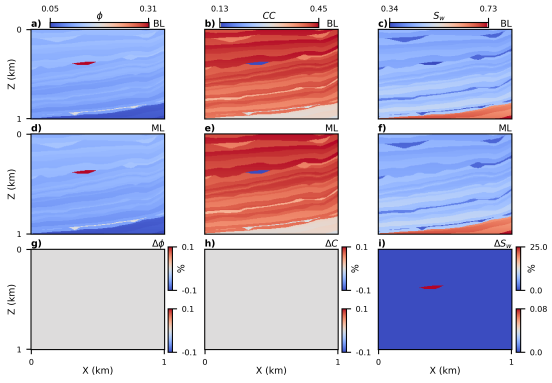

Figure 1: True (a-c) baseline and (d-f) monitor models with PCS parameterization. (g-i) The difference between two models which are shown with two color scales. The upper color scale represents the absolute value of differences in percent while the lower color scale presents the changes in typical unit of each parameter.

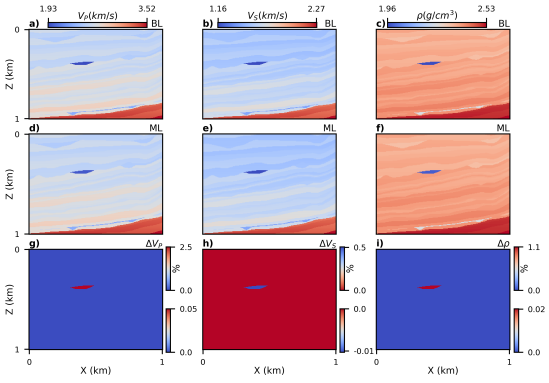

Figure 2: True (a-c) baseline and (d-f) monitor models with DV parameterization. (g-i) The difference between two models which are shown with two color scales. The upper color scale represents the absolute value of difference in percent while the lower color scale presents the changes in typical unit of each parameter as shown above the first row.

carried out using multiscale strategy (Bunks et al., 1995) with frequencies of 10, 20, 25, 35, 40, and 55 Hz. The ℓ-BFGS method (Nocedal and Wright, 2006) updates an initial model through 10 iterations for each frequency. In this study, we used a smoothed version of the baseline, Figure 1, as the initial model for both FWI and TL-FWI (Figure 3(a-c)).

After estimating the porosity and clay content (Figure 3(d-g)), these two parameters and the initial S_w are imported to the TL-FWI algorithm and by considering $\lambda_\Delta = 1\times10^{-6}$, the time-lapse result is obtained as Figure 3(h). Besides, by skipping the first FWI and using the initial model (Figure 3(a-c)) as the input of TL-FWI, we can obtain a noisier but still interpretable estimate of time-lapse water saturation as presented in Figure 3(i). For a better comparison, a 1D estimate of both approaches are presented in Figure 3(j) where the values are obtained alongside an imaginary well that passes the reservoirs at $X = 390$ m.

CONCLUSIONS

In this study, the formulation for direct estimation of the rock-physics properties using FWI and Gassmann's equation is presented. We discussed why time-lapse full-waveform inversion is more challenging with DV parameterization. By performing time-lapse full-waveform inversion with PCS parameterization, we can accumulate all time-lapse changes in one model parameter leading to a less challenging problem by reducing parameter crosstalk.

We showed that the initial model has a large impact on TL-FWI and that a good estimation of porosity and clay content allows obtaining cleaner results. This can be achieved by performing a multiparameter FWI on the baseline survey prior to saturation monitoring with TL-FWI.

APPENDIX A

APPENDIX A: GRADIENT OF COST FUNCTION IN PCS PARAMETERIZATION

Considering P as ϕ, vector $\mathbf{b}$ in equation 8 is built by

$$\frac{\partial K}{\partial \phi} = \frac{k_D + \phi\frac{\partial K_D}{\partial \phi} - \frac{K_f}{k_s}\left(K_D + (1+\phi)\frac{\partial K_D}{\partial \phi}\right)}{\phi(1+\Delta)} - \frac{\left[\phi K_D + \left(1 - \frac{(1+\phi)K_D}{K_s}\right)K_f\right]\left(1+\Delta+\phi\frac{\partial \Delta}{\partial \phi}\right)}{\phi^2(1+\Delta)^2},$$
$$\frac{\partial \mu}{\partial \phi} = -\mu_s\frac{1+\frac{3}{2}cs}{(1+\frac{3}{2}cs\phi)^2}, \qquad \text{(A-1)}$$
$$\frac{\partial \rho}{\partial \phi} = \rho_f - \rho_s,$$

where

$$\frac{\partial K_D}{\partial \phi} = -K_s\frac{1+cs}{(1+cs\phi)^2}, \qquad \text{(A-2)}$$

and

$$\frac{\partial \Delta}{\partial \phi} = -\frac{K_f}{K_s\phi^2}\left(1 - \frac{1}{1+cs\phi}\right) + \frac{K_f(1-\phi)}{K_s\phi}\frac{cs}{(1+cs\phi)^2}. \qquad \text{(A-3)}$$

With respect to C, we have

$$\frac{\partial K}{\partial C} = \frac{\phi\frac{\partial K_D}{\partial C} + \frac{K_f(1+\phi)}{K_s^2}\left(\frac{\partial k_s}{\partial C}k_D - \frac{\partial k_D}{\partial C}k_s\right)}{\phi(1+\Delta)} - \frac{\left[\phi K_D + \left(1 - \frac{(1+\phi)K_D}{K_s}\right)K_f\right]\phi\frac{\partial \Delta}{\partial C}}{\phi^2(1+\Delta)^2},$$
$$\frac{\partial \mu}{\partial C} = \frac{1-\phi}{1+\frac{3}{2}cs\phi}\frac{\partial \mu_s}{\partial C}, \qquad \text{(A-4)}$$
$$\frac{\partial \rho}{\partial C} = (1-\phi)(\rho_c - \rho_q),$$

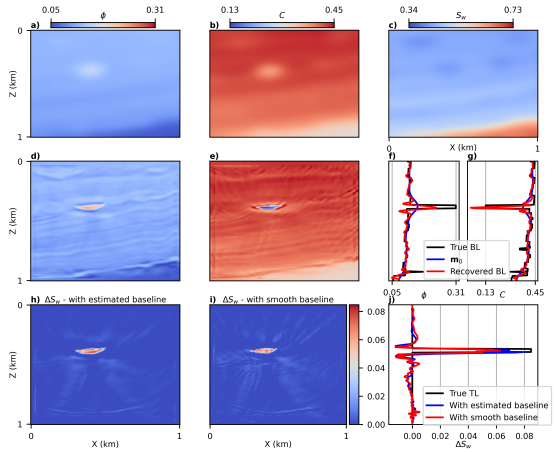

Figure 3: (a-c) The initial model in PCS parameterization. (d-g) The recovered porosity and clay content for baseline. (h-j) Estimated time-lapse image of water saturation.

where

$$\begin{aligned}\frac{\partial K_s}{\partial C} &= K_c - K_q,\\ \frac{\partial \mu_s}{\partial C} &= \mu_c - \mu_q,\\ \frac{\partial K_D}{\partial C} &= \frac{1-\phi}{1+cs\phi}\frac{\partial K_s}{\partial C},\end{aligned} \tag{A-5}$$

and

$$\frac{\partial \Delta}{\partial C} = \frac{(\phi-1)K_f}{\phi K_s^2}\left(1-\frac{1}{1+cs\phi}\right)\frac{\partial K_s}{\partial C}. \tag{A-6}$$

The subscripts c and q present the property of clay and non-clay materials in rock. Finally, for S_w, we have

$$\begin{aligned}\frac{\partial K}{\partial S_w} &= \frac{\left(1-\frac{(1+\phi)K_D}{K_s}\right)\frac{\partial K_f}{\partial S_w}}{\phi(1+\Delta)} - \\ &\quad \frac{\left[\phi k_D + \left(1-\frac{(1+\phi)K_D}{K_s}\right)K_f\right]\phi\frac{\partial \Delta}{\partial S_w}}{\phi^2(1+\Delta)^2},\\ \frac{\partial \mu}{\partial S_w} &= 0,\\ \frac{\partial \rho}{\partial S_w} &= \phi(\rho_w - \rho_h),\end{aligned} \tag{A-7}$$

where

$$\begin{aligned}\frac{\partial k_f}{\partial S_w} &= k_w - k_h,\\ \frac{\partial \Delta}{\partial S_w} &= \frac{\Delta}{k_f}\frac{\partial k_f}{\partial S_w}.\end{aligned} \tag{A-8}$$

ACKNOWLEDGMENT

This project was supported by a NSERC Discovery Grant to BG (RGPIN-2017-06215). The authors thank Qi Hu for providing the Marmousi model in PCS parameterization as used for the baseline model.

References

Bunks, C., F. M. Saleck, S. Zaleski, and G. Chavent, 1995, Multiscale seismic waveform inversion: Geophysics, **60**, no. 5, 1457–1473, doi: https://doi.org/10.1190/1.1443880.

Dupuy, B., S. Garambois, and J. Virieux, 2016, Estimation of rock physics properties from seismic attributes — part 1: Strategy and sensitivity analysis: Geophysics, **81**, no. 3, M35–M53, doi: https://doi.org/10.1190/geo2015-0239.1.

Fabien-Ouellet, G., E. Gloaguen, and B. Giroux, 2017, Time-domain viscoelastic full-waveform inversion: Geophysical Journal International, **209**, no. 3, 1718–1734, doi: https://doi.org/10.1093/gji/ggx110.

Gassmann, F., 1951, Uber die elastizitat poroser medien: Vierteljahrsschrift der Naturforschenden Gesellschaft in Zurich, **96**, 1–23.

Hu, Q., S. Keating, K. A. Innanen, and H. Chen, 2021, Direct updating of rock-physics properties using elastic full-waveform inversion: Geophysics, **86**, no. 3, MR117–MR132, doi: https://doi.org/10.1190/geo2020-0199.1.

Landrø, M., H. H. Veire, K. Duaut, and N. Najjar, 2003, Discrimination between pressure and fluid saturation changes from marine multicomponent time-lapse seismic data: Geophysics, **68**, no. 5, 1592–1599, doi: https://doi.org/10.1190/1.1620633.

Lang, X., and D. Grana, 2019, Rock physics modelling and inversion for saturation-pressure changes in time-lapse seismic studies: Geophysical Prospecting, **67**, 1912–1928, doi: https://doi.org/10.1111/1365-2478.12797.

Lumley, D. E., 1996. Seismic time-lapse monitoring of subsurface fluid flow: Stanford University.

Ma, Y., M. Maharramov, R. Clapp, and B. Biondi, 2016, Multiparameter full-waveform inversion in the isotropic acoustic media with application to time-lapse seismic inverse problem: 86th Annual International Meeting, SEG, Expanded Abstracts, 5557–5561, doi: https://doi.org/10.1190/segam2016-13879808.1.

Maharramov, M., and B. Biondi, 2014, Robust joint full waveform inversion of time-lapse seismic data sets with total-variation regularization: arXiv:1408.0645.

Mardan, A., B. Giroux, and G. Fabien-Ouellet, 2022a, PyFWI: A python package for full-waveform inversion (FWI).

Mardan, A., B. Giroux, and G. Fabien-Ouellet, 2022b, Time-lapse seismic full waveform inversion using improved cascaded method: 2nd EAGE Conference on Seismic Inversion, EAGE, 1–5, doi: https://doi.org/10.3997/2214-4609.202229003.

Mavko, G., T. Mukerji, and J. Dvorkin, 2020, The rock physics handbook: Cambridge University Press.

Nocedal, J., and S. J. Wright, 2006, Numerical optimization: Springer.

Pride, S., 2005, Hydrogeophysics: Water science and technology library: Springer.

Queißer, M., and S. C. Singh, 2013, Full waveform inversion in the time-lapse mode applied to CO_2 storage at Sleipner: Geophysical Prospecting, **61**, 537–555, doi: https://doi.org/10.1111/j.1365-2478.2012.01072.x.

Tarantola, A., 1986, A strategy for nonlinear elastic inversion of seismic reflection data: Geophysics, **51**, no. 10, 1893–1903, doi: https://doi.org/10.1190/1.1442046.

Zhou, W., and D. Lumley, 2021, Central-difference timelapse 4D seismic full-waveform inversion: Geophysics, **86**, no. 2, R161–R172, doi: https://doi.org/10.1190/geo2019-0834.1.